Chemical Engineering Research and Design 206 (2024) 54–61

Contents lists available at ScienceDirect

Chemical Engineering Research and Design

journal homepage: www.elsevier.com/locate/cherd

Effect of the kinematic viscosity on liquid flow hydrodynamics in vortex mixers

Gozde GECIM [a], Ertugrul ERKOC [a,b,*]

[a] Department of Chemical Engineering, Faculty of Engineering and Natural Sciences, Bursa Technical University, Bursa, Turkey
[b] Admire-Tech Inc., Bursa, Turkey

ARTICLE INFO

Keywords:
Vortex mixer
Liquid flow hydrodynamics
Similar liquids
PIV
PLIF

ABSTRACT

The effect of the kinematic viscosity of similar fluids on liquid flow hydrodynamics and the onset of the instability were investigated to acquire information on the mixing behavior of vortex mixers. To assess the influence of the kinematic viscosity, water and two glycerin aqueous solutions with varying weight percentages (25 wt % and 50 wt %) were used. The critical Reynolds number of the flow regime transitions was found using PLIF and PIV flow-field techniques. The liquid flow hydrodynamics and gas flow dynamics in the proposed vortex mixer geometry were compared, as well. It was observed that the kinematic viscosity has a linear relation with the critical Reynolds number; however, the coefficient is different for liquids and gases. Additionally, kinematic viscosity dictates the minimum Reynolds number where the fluids have a full turn inside the chamber. It was observed that fluids having higher kinematic viscosities have a full turn at lower Reynolds numbers, and the critical Reynolds number value decreases with increasing kinematic viscosity.

1. Introduction

Jet mixing devices offer an alternate method for fluid mixing, particularly at low Reynolds numbers where mixing is solely based on molecular diffusion (Xia and Zhong, 2013). They are commonly utilized as fast mixing devices owing to their high mass and heat transfer rates and mixing efficiency values (Alboiu et al., 2017). Jet mixers are employed in a variety of industrial applications, such as chemical production and polymer processing, as well as drying solid particles and blending non-Newtonian fluids (Jin and Cao, 2022; Valdés et al., 2022).

Confined impinging jets (CIJs) and T-jets, which have opposed cylindrical/square jets and an impingement region to offer increased mixing, are the most commonly employed jet mixers. This impingement region is known to be stretched and folded by shear forces, promoting mixing (Bie et al., 2022). While CIJs are used for the mixing of both low and high viscosity fluids, T-jets are generally preferred for only low viscosity fluids (Li et al., 2022).

Flow visualization techniques, such as optical and laser techniques, are commonly used to gain a fundamental understanding of mixing flow hydrodynamics in CIJs or T-jets (Hoffmann et al., 2006; Shen et al., 2022). The transition between flow regimes can be associated with the determination of the critical Reynolds (Re)number of the flow where the flow regime changes from steady to unsteady. The mixing quality is known to be strongly dependent on flow regimes (Jin and Cao, 2022).

Recently, the effect of operational and design parameters on the mixing hydrodynamics for CIJs and T-jets has been revealed by the critical Reynolds number characterization. In CIJs, a segregated flow regime is observed at Re = 100 where axial flow is formed, and the mixing chamber is divided in half by the steady parallel flow of both jets. The critical Re number of this system was determined to be Re = 120 as the turbulence intensity is doubled. This flow regime is also known as a vortex flow regime due to the helicoidal movement of vortices inside the jets and their rotation along the mixing chamber axis (Li and Xu, 2023; Sultan et al., 2012). At Re = 200, a self-sustainable chaotic regime in which downstream vortices are formed and the segregation inside the flow decreases due to the radial oscillation of the jets. As the intensity of segregation decreases in this chaotic flow regime, mixing indexes increase (Li and Xu, 2023; Sultan et al., 2012). When Re number increased to 500, axial oscillations rather than radial oscillations were observed. At even higher Re numbers, flow regime becomes more unstable and vortex shedding is defined as an effective mixing regime where the counter-rotating vortices promote fast mixing (Brito et al., 2022b; Li et al., 2014; Santos et al., 2008).

The effect of Reynolds number on flow regime has also been studied

* Corresponding author at: Department of Chemical Engineering, Faculty of Engineering and Natural Sciences, Bursa Technical University, Bursa, Turkey.
E-mail addresses: gozde.salkic@btu.edu.tr (G. GECIM), ertugrul.erkoc@btu.edu.tr (E. ERKOC).

https://doi.org/10.1016/j.cherd.2024.04.034
Received 29 November 2023; Received in revised form 25 March 2024; Accepted 15 April 2024
Available online 20 April 2024

for T-jets. In conventional T-jets, flow hydrodynamics for similar liquids is divided into three flow regimes known as the stratified flow regime ($Re \leq 136$), the vortex flow regime ($Re \geq 136$) and the engulfment flow regime ($Re \cong 200$) (Ansari et al., 2018). Mixing at low Re numbers as in stratified flow regime is slow since it is diffusion controlled. On the other hand, at high Re numbers (in vortex and engulfment flow regimes), fluid streams encounter a larger surface area but a smaller diffusion distance, which results in shorter diffusion time and better mixing performance (Andersson et al., 2011; Ansari et al., 2018; Camarri et al., 2020; Mariotti et al., 2020). In addition to the studies on similar liquids, Mariotti et al. (Mariotti et al., 2020) investigated the effect of the mixing performance of methylene blue and ascorbic acid on the methylene blue reduction reaction. Similar flow regimes were noted, however stratified and vortex flow regimes showed stratification effects as a result of fluid density differences. As the convection mechanism becomes more pronounced than the diffusion mechanism, these effects decrease in the engulfment flow regime. Liquid mixing hydrodynamics was investigated for nonaligned T-jet reactors in addition to conventional T-jet geometries (Ansari et al., 2012; Camarri et al., 2020; Chan et al., 2019; Rabani et al., 2016; Zhang et al., 2020). The flow regime is divided into three regions: stratified flow regime ($Re < 40$), steady engulfment regime ($40 < Re < 215$), and unsteady engulfment regime ($Re > 215$) (Zhang et al., 2020). For the liquid flow hydrodynamics, a T-T jet reactor with four opposing jets was also investigated. It provided better mixing performance than the conventional T-jet reactor as a result of increased vortex structure and contact surface area. Because it is primarily dependent on diffusion, it ultimately results in enhanced mixing in even segregated flow regimes. The segregated and vortex flow regimes were observed at $Re < 140$, while the unsteady engulfment flow was formed at $140 < Re < 400$(Bie et al., 2022).

Whether the jets are opposed as in T-jets and CIJs, or angled, as in V-type or arrow-type reactors, the hydrodynamics of impinging jets are dependent on the momentum ratio of the jets. This can constrain the design of the geometry due to the differences or competition between the jets. Furthermore, the balance of the opposed jets, which means the impingement point should be in the center of the chamber, is required. Otherwise, inefficient mixing conditions in the opposed jets occur, leading to increased manufacturing costs and operational problems (Brito et al., 2022a). Thus, vortex mixers with tangentially opposed jets where the equal momentum of the jets is not critical can be advantageous for applications requiring fast mixing (Cheng et al., 2009; Shi et al., 2011). These mixers offer swirling flow in the mixing chamber due to the formation of centrifugal force, creating pressure gradients in the radial direction. As a result, mixing efficiency improves (Li et al., 2022; Wu et al., 2021).

Vortex mixers can have a great potential in chemical industries using gas-solid or liquid-solid catalyst systems, whether in small dimensions or in bigger dimensions (Gecim and Erkoc, 2022). For liquid processes, vortex mixers including two or more jets are widely used in nano-precipitation reactions where fast mixing is required (Liu et al., 2015).

In this study, flow hydrodynamics for similar liquids in a vortex mixer geometry is presented. While a great deal of research has been done on the liquid flow hydrodynamics in CIJs or T-jets, there is still a lack of knowledge about vortex mixers (Li et al., 2014; Santos et al., 2008). The geometry of the vortex mixer presented here is similar to that of multi-inlet vortex reactors (MIVR) where multiple jets are used (Hitimana et al., 2019). The formation of velocity fluctuations in MIVRs causes a decrease in boundary layer thickness and an increase in the steady interaction between phases due to the swirling nature of the flow. Effective mass and heat transfer are thus obtained (Liu et al., 2014; Xiang et al., 2017).

Gas flow dynamics in the presented vortex mixer geometry was previously studied by our group (Gecim and Erkoc, 2021, 2022). Smoke-seeded flow is concentrated in one part of the chamber at $Re < 70$, according to experiments on gas flow in vortex mixers. This flow regime is called stratified flow as a certain segregation of fluid streams cannot be observed. At $Re = 70$, smoke seeded flow completes a full rotation of the chamber, which is known as the vortex flow regime. As the Re number increases, radial and axial oscillations occur in the flow. The critical Re number is defined as the point at which the balance between these oscillations is broken and the flow becomes irregular. This is also known as the onset of the unsteady flow regime, and as Re number increases, the flow evolves to the chaotic regime (Gecim and Erkoc, 2021).

In a recent work, our group presented the effect of kinematic viscosity on the critical Re number for gas flow dynamics when employing the vortex mixer design provided. It was found that gases with higher kinematic viscosities will have a single defined vortex at lower Reynolds numbers and the formation of a full vortex in the channel is governed by the momentum rate of the jets, which is the function of gas property (density) and velocity (Gecim and Erkoc, 2022). The present study aims to reveal liquid flow hydrodynamics and determine the effect of kinematic viscosity for the presented vortex mixer geometry. Liquid flow hydrodynamics were investigated by PLIF and PIV experiments to characterize the flow field and turbulent parameters in the mixing chamber with respect to liquid physical properties.

2. Experimental methods

2.1. Vortex mixer

Vortex mixer used in this work has a typical geometry which was employed in our recent gas flow dynamic studies. Fig. 1 shows the 3D vortex mixer geometry with a D_c/D_{inj} ratio of 2 (where D_c is the diameter of the chamber and D_{inj} is the diameter of the injectors). A detailed explanation of the mixer was given in our recent works, as well (Gecim and Erkoc, 2021, 2022).

To assess the hydrodynamics of the similar liquids in the vortex mixer reactor, three sets of experiments including *water/water* and $glycerin^{aq}/glycerin^{aq}$ solutions (with weight percentages of 25 % and 50 %) were performed. The physical properties of glycerin aqueous solutions in room conditions were determined using the general expressions for density and dynamic viscosity (Santos et al., 2008). Kinematic viscosity values were calculated from the ratio of dynamic viscosity over density. Table 1 summarizes the physical properties of the liquids.

The desired flow rate of the liquids was controlled by flow controllers (Coriflow) where they were supplied from the tanks using the pumps. The evolution of liquid flow hydrodynamics was performed based on the flow regime transitions where the flow changes from steady to unsteady. This was examined based on the Re number of the jets between $Re = 30$ and $Re = 280$ with intervals of $Re = 10$ for each experiment. Thus, the critical Re numbers for liquids with different physical properties were established to determine the onset of the unsteady flow regime.

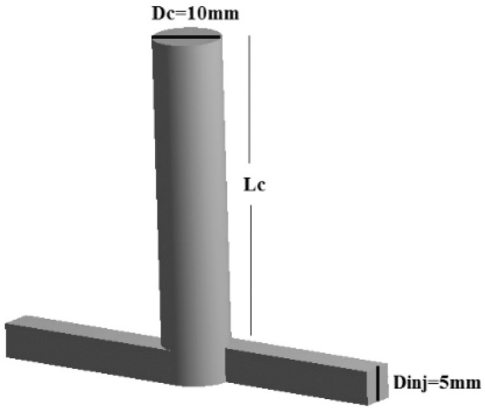

Fig. 1. 3D view of the vortex reactor.

Table 1
Fluid properties at experimental conditions.

	ρ(kg/m^3)	μ (kg/m.s)	ν (m^2/s)
Water	996.0	9.59E-04	9.63E-07
Glycerin^{aq} (25.0 wt %)	1062.3	2.12E-03	2.00E-06
Glycerin^{aq} (50.0 wt %)	1128.4	5.65E-03	5.49E-06

2.2. PLIF and PIV setup and measurements

A vortex mixer experimental setup similar to that used in the gas flow hydrodynamics study was used for the PLIF and PIV experiments. The description of the vortex mixer experimental setup for gas flow hydrodynamics has been previously done in great detail by our group (Gecim and Erkoc, 2021, 2022). For both flow visualization and PIV experiments, a CMOS camera (Speedsense 1040) with 2330×1723 megapixels resolution and frame rate of 30 Hz was used to capture the frames lighted by each laser flash. The laser source used is a double laser head from Dantec Dynamics™ (Nd-YAG laser (532 nm, 50 mj) at a frequency of 96 Hz.

To visualize the liquid flow and determine the flow regime transitions, PLIF experimental technique was used (Fig. 2). With this technique, one of the incoming liquid flows was introduced with a fluorescent substance, and the other one was a clear liquid. Rhodamine 6 G was chosen as the fluorescent dye as it has the maximum absorption of light close to 525 nm enabling excitation with 532 nm from Nd-YAG laser. It also emits fluorescence at 555 nm which is at a different wavelength from the laser (532 nm) (Crimaldi, 2008). A bandpass filter was applied to the laser source of the experimental setup to ensure visibility. The concentration of the Rhodamine 6 G was determined based on the literature where the flow structures are visible (3.5×10^{-4} g/l) (Sultan et al., 2012). The PLIF setup and image acquisition were made with Dantec Dynamics™. The average behavior of the flow in both stable and unstable regimes was observed with the root mean square (rms) method, which considers the standard deviation of the corresponding pixels from their mean value.

In the gas flow dynamics experiments, radial planes along the chamber height with 10 mm intervals starting from the bottom were analysed in great detail (Gecim and Erkoc, 2021, 2022). The gas flow dynamics was found to develop at $10mm < L_c < 40mm$. Thus, PLIF experiments for the liquid flow hydrodynamics study were performed for the radial plane of chamber height at 30 mm, which is defined as plane-3.

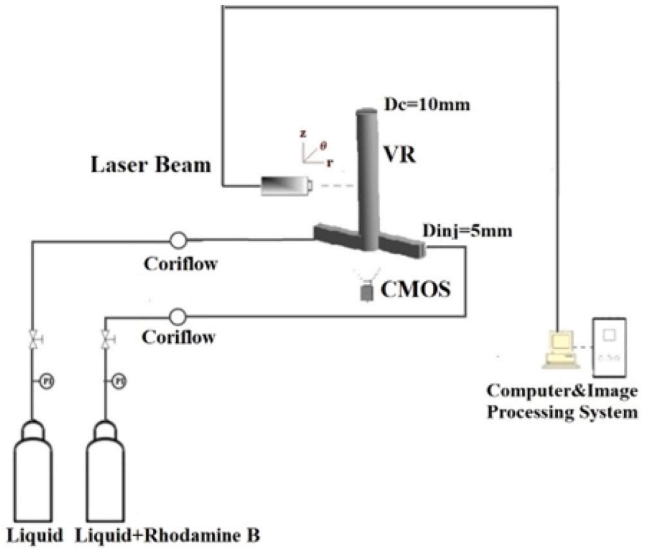

Fig. 2. Vortex mixer PLIF experimental setup.

Following this, PIV experiments were applied to reveal the flow field characteristics of the liquid/liquid mixing in the presented vortex mixer geometry. For the PIV experiments, to obtain the liquid flow field and turbulent characteristics, one of the incoming liquid flows was seeded with polyamide seeding particles and the other one was a clear liquid. The diameter of the polyamide seeding particles is about 5 μm which is small enough to neglect its effect on the fluid flow. The displacement of the polyamide seeding particles between two frames captured in pairs gave the 2D liquid flow field in the vortex mixer. The number of images was optimized for the post processing time in our previous studies (Gecim and Erkoc, 2021, 2022). A time average of 512 pictures was compared to the time average of 128 pictures. The time averaged results were the same, so 128 pictures were found to be sufficient. A multipass (total of 8 passes) PIV algorithm, with a decreasing interrogation window from 128×128 to 32×32 was applied. Time interval between two frames, dt, was taken as 5164 μs. The velocity vectors were calculated from the displacement of seeding particles between two subsequent frames. The Adaptive PIV method, which was thoroughly detailed in our most recent work, was used to disclose the liquid flow hydrodynamics in the presented vortex mixer geometry (Santos et al., 2008).

3. Results and discussion

The time-averaged flow visualization images from radial flow visualization experiments performed at a chamber height of 30 mm were demonstrated in Fig. 3. While the white color in the PLIF images represents one of the incoming jets dyed with rhodamine 6 G which emits fluorescence in the presence of the laser; the dark color belongs to the clear liquid. It is clear that until around Re = 30, the jets don't have enough force to have a full turn in the chamber, hence the segregation of two jets can be observed. For pure water and glycerin aqueous solution of 25 wt %, the vortex flow behavior was gained at Re = 40, and the flow developed similarly until Re = 130. Nonetheless, compared to water, the observed rotation number of the vortex behavior for glycerin aqueous solution of 25 wt % is higher than that of water. The kinematic viscosity of the glycerin solution is higher, and thus the liquid velocity of the jets at the same Re numbers is two times higher than that of water. This causes the flow hydrodynamics of glycerin aqueous solution of 25 wt % to grow faster than water.

For glycerin aqueous solution of 50 wt %, the formation of vortex flow behavior was observed at Re = 30. Moreover, the flow looks like it evolves differently than the others, as the fluid streamlines are intertwined even at low *Re* numbers (Re = 50 − 60). This can be attributed to the high viscous forces of the glycerin aqueous solution of 50 wt %. It has the highest dynamic viscosity and hence the highest kinematic viscosity of all. The mixing of two incoming jets seems to be completed from the time-averaged results of the PLIF images for the glycerin aqueous solution of 50 wt %.

The evolution of flow structures for water and glycerin aqueous solutions has been analyzed from time averaged flow visualization images. Although the first turning points of the liquid flows have been easily determined with respect to the time averaged results, it is important to analyze the instantaneous flow behaviors to determine the critical Re number of the flow where a radical dramatic change in the flow hydrodynamics occurs. From Fig. 4a, it can be seen that liquid flow streamlines disappeared beyond Re ≥ 220, and the vortex behavior of the flow became almost unnoticeable for water flow. After this point, shortened fluid streams occur and the thickness of the boundary layer decreases. Thus, during this regime, convection becomes more prominent than diffusion resulting in enhanced mass and heat transfer rates (Supporting Information video 1 and video 2). Although the flow hydrodynamics of Glycerin^{aq} (25 wt %) evolves in the same way with water flow at lower Re numbers, the flow regime changes from steady to unsteady starting at Re = 200 (Fig. 4b) (Supporting Information video 3 and video 4). Additionally, the critical Re number of Glycerin^{aq} (50 wt %) is defined at around Re = 170 from the flow visualization

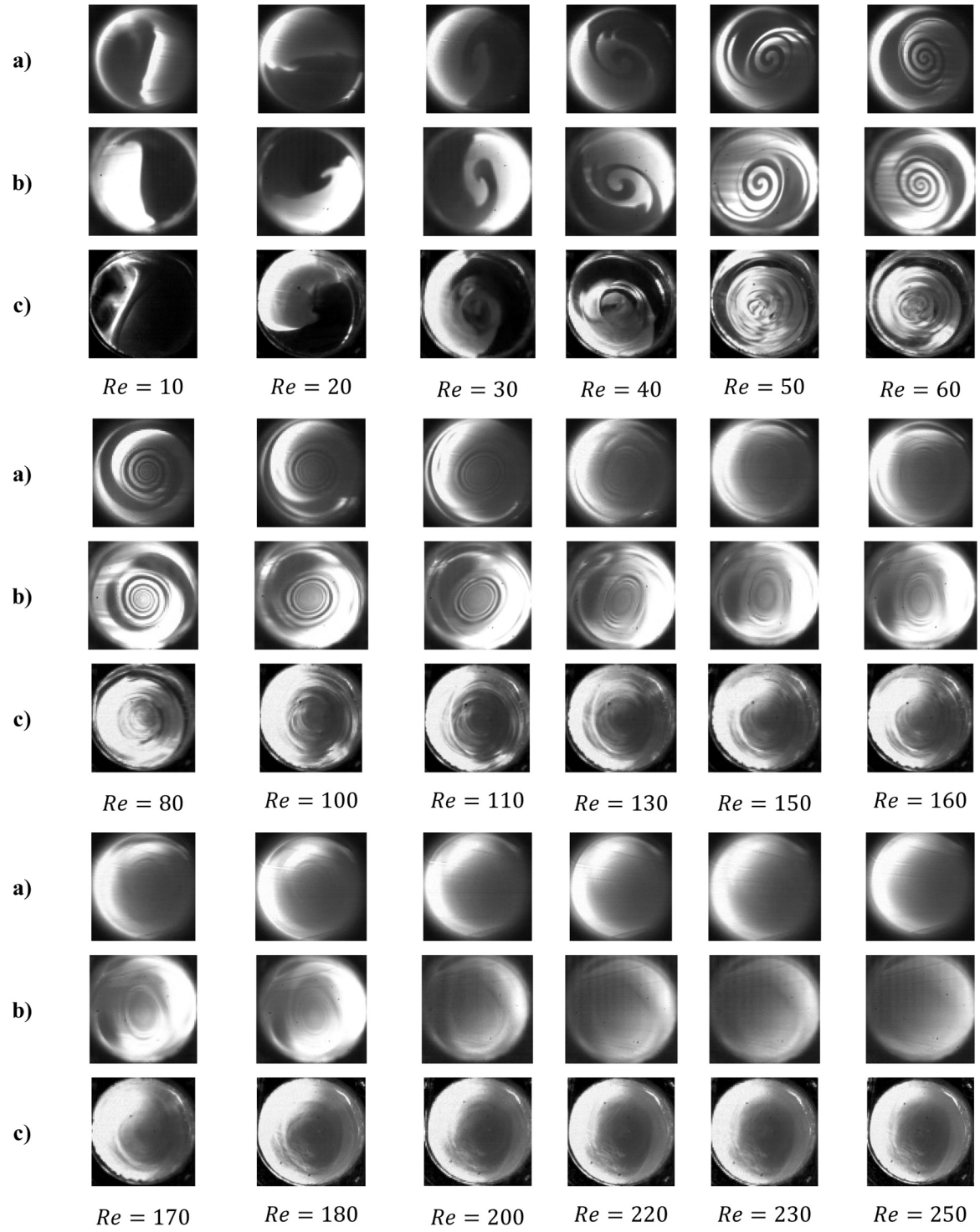

Fig. 3. Time-averaged flow images at plane-3 a) Water b) Glycerin^{aq} (25 wt %) c) Glycerin^{aq} (50 wt %).

experiments (Supporting Information video 5 and video 6). As the weight of the glycerin increases in the aqueous solution, the average kinematic viscosity of the solution increases as shown in Table 1. It can be concluded from both time-averaged and instantaneous results, that flow regime changes from steady to unsteady at lower Re numbers for the liquids with higher kinematic viscosities.

Supplementary material related to this article can be found online at

In this regard, Table 2 summarizes the three liquid flow regime regions identified in the vortex mixer: the stratified flow regime, the vortex flow regime, and the unsteady engulfment regime. While the mixing is mainly dependent on the diffusion at stratified flow, it becomes dependent on the convection due to the axial instabilities created by the tangential characteristics of the jets. At stratified flow regime, there is a clear symmetry of the incoming liquid flows where a small amount of mass transfer occurs. As Re number increases, incoming gas flows show a vortex profile inside the chamber due to the tangential behavior of the jets. During this regime, mixing is dependent on both diffusion and convection. However, for larger Re numbers, mixing quality is known to be increased in unsteady engulfment flow regime where the intertwined structures of fluid streams cause high

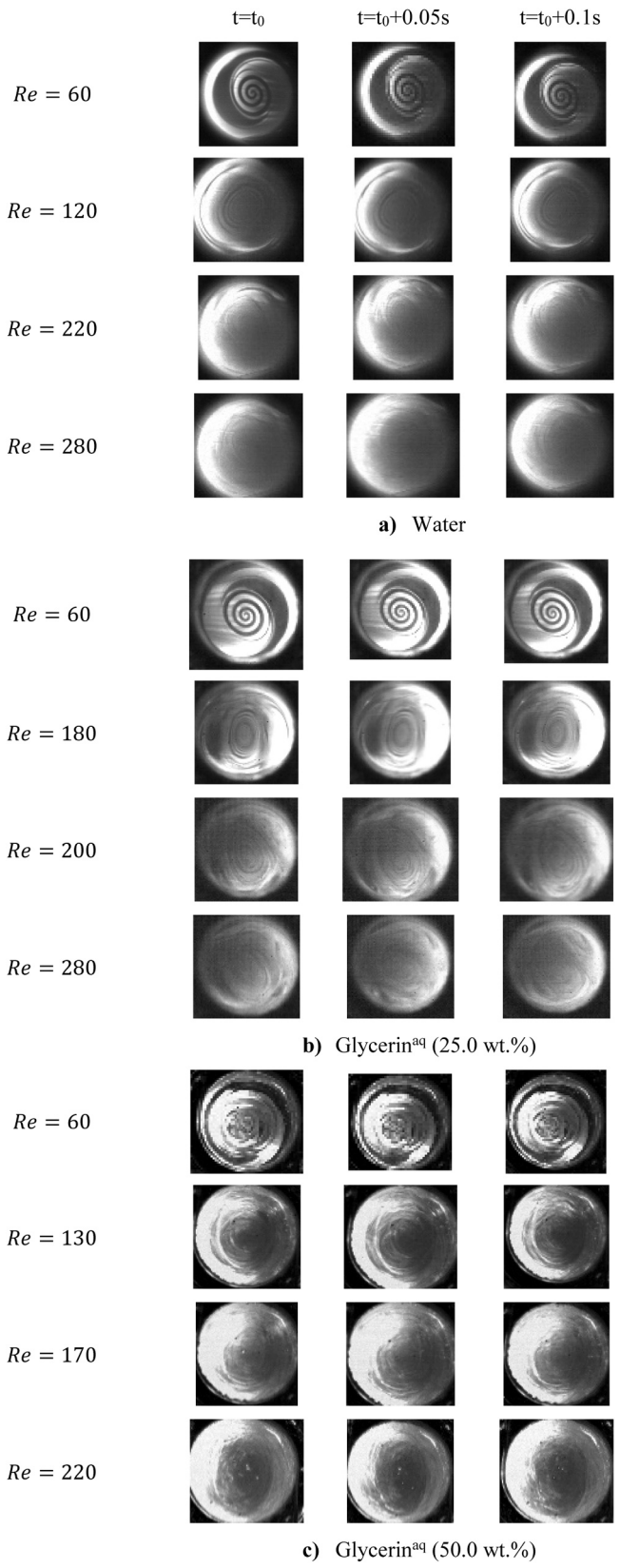

Fig. 4. Instantaneous flow images at plane-3 a) Water b) Glycerin^{aq} (25 wt %) c) Glycerin^{aq} (50 wt %).

Table 2
Flow regime transitions.

	Stratified Flow Regime	Vortex Flow Regime	Unsteady Engulfment flow regime
Water	Re < 40	40 ≤ Re < 220	Re ≥ 220
Glycerin^{aq} (25.0 wt %)	Re < 40	40 ≤ Re < 200	Re ≥ 200
Glycerin^{aq} (50.0 wt %)	Re < 30	30 ≤ Re < 170	Re ≥ 170

concentration gradient with shorter thickness of boundary layer.

As mentioned earlier, the gas flow dynamics of similar gases with different kinematic viscosities has been revealed by our group. In Fig. 5, the critical Re number of the liquid and gas flows in the presented vortex mixer geometry is compared. The decreasing trend of the Re_c based on the increasing kinematic viscosity is found to be similar for liquid and gas flows. Re_c was found to be very close for three gases, namely methane, argon, and nitrogen, due to their close kinematic viscosity values (Gecim and Erkoc, 2021, 2022). Thus, the linear relationship between Re_c and kinematic viscosity is more pronounced for liquids. Additionally, the calculated coefficients of trendlines for liquids and gases were shown to be different. The operating Re number of the proposed vortex mixer design to ensure efficient mixing may be precisely established for the liquids and gases with the range of kinematic viscosity that is supplied.

From the PIV measurements, time-averaged flow field characterizations were performed by the formation of velocity vector maps for the determined points of the flows. Fig. 6 depicts the time averaged flow field for the selected Re numbers before and after the critical Re numbers for water and glycerin aqueous solutions. It can be deduced that the tangential flow of coming jets through the chamber walls is the main characteristic of the liquid flow, and this behavior was preserved along the chamber length. As the *Re* number increases, vortex wandering motion of the flow around the center axis is clearly noticeable. Liquids with higher kinematic viscosities have a full vortex rotation at lower Re numbers, much like gases do. In the previous study of our group, a detailed explanation of forces acting on the fluid particles is given (Gecim and Erkoc, 2022). The balance between pressure forces and viscous forces is known to be broken at this point called the critical point of the flow which can also be called the onset of the unsteady flow regime. For the liquids with higher kinematic viscosities, the balance between centrifugal forces and the pressure gradients acting on the flow breaks earlier. Thus, the flow hydrodynamics of glycerin aqueous solution of 50 wt % evolve earlier than that of water and glycerin aqueous solution of 25 wt %.

The instantaneous velocity profiles below and above critical Reynolds numbers acquired from PIV experiments are shown in Fig. 7, where they are plotted on a radial line that passes through the origin at the rø plane (bottom plane). The velocity profile from the origin to the half of the chamber displays the classical profile of a forced vortex at the steady state, below the critical Reynolds numbers, where the velocities in the center are zero. That is, the velocity changes linearly with the radius until the half of the chamber from both sides. There is evidence of a laminar flow profile between the chamber's wall and half. A detailed discussion of the forces operating on the fluid particles was provided in our group's previous paper, which examined similar gas flow dynamics in the vortex mixer that was presented (Gecim and Erkoc, 2022). In summary, it was found that the critical point of the flow is the point at which the equilibrium between viscous and pressure forces with the centrifugal force is disrupted. This point can also be referred to the start of unsteady flow regime. As illustrated in Figure 12, the instantaneous velocity profiles exhibit relative motion with regard to the rotating frame of reference and acceleration (changes in local velocities with time) at their critical points, where the centrifugal force is no longer able to balance the pressure gradient force.

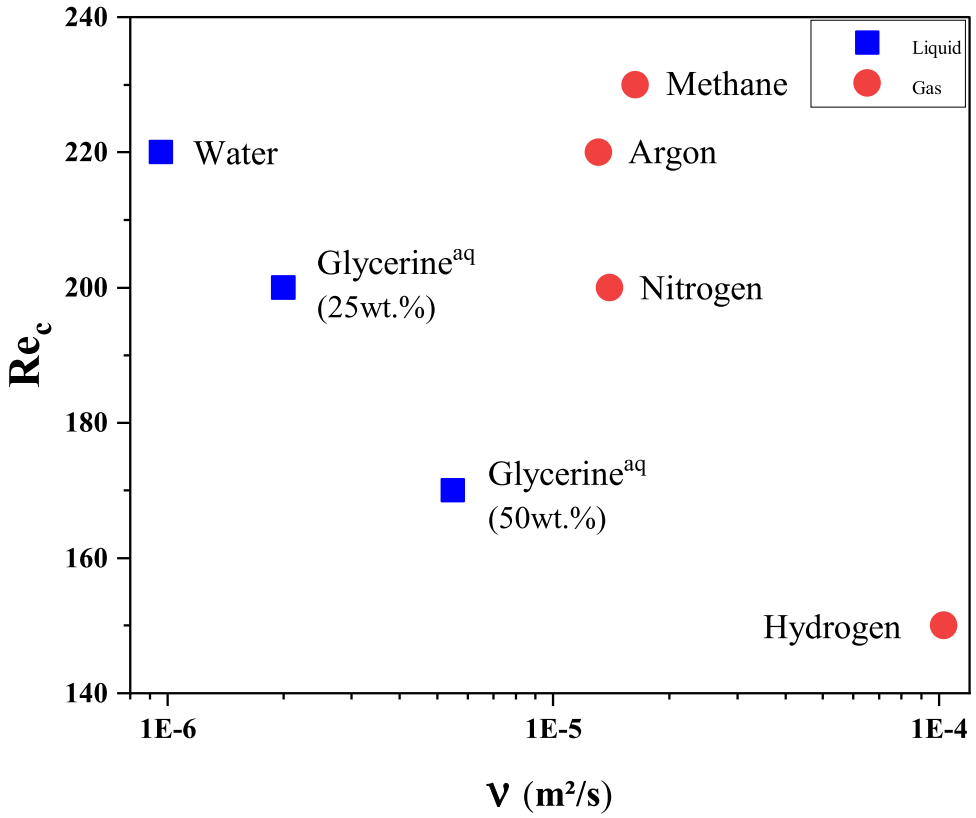

Fig. 5. The effect of kinematic viscosity on the critical Re number.

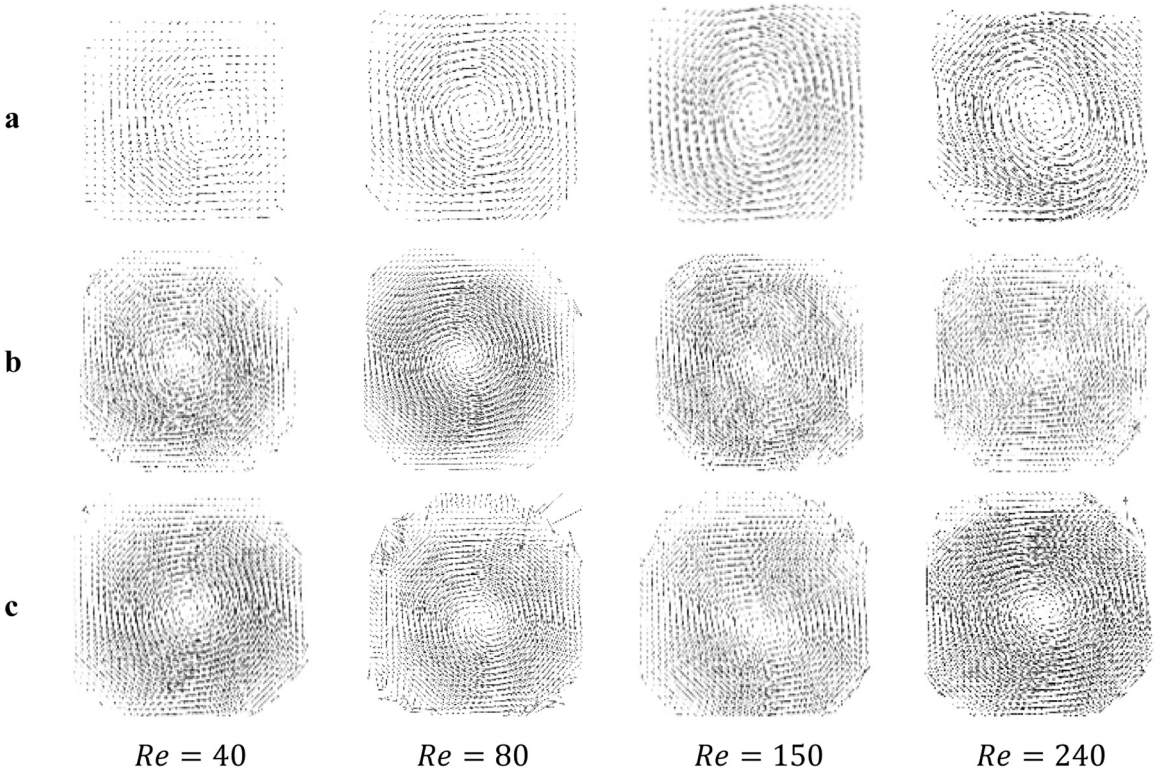

Fig. 6. Time-averaged velocity vectors of determined flow regime regions a) Water b) Glycerin^{aq} (25 wt %) c) Glycerin^{aq} (50 wt %).

4. Conclusions

To successfully reveal the design characteristics of vortex mixers, it is important to examine both liquid flow hydrodynamics and gas flow dynamics. In the presented study, the effects of liquid properties on the flow hydrodynamics were characterized in the proposed vortex mixer

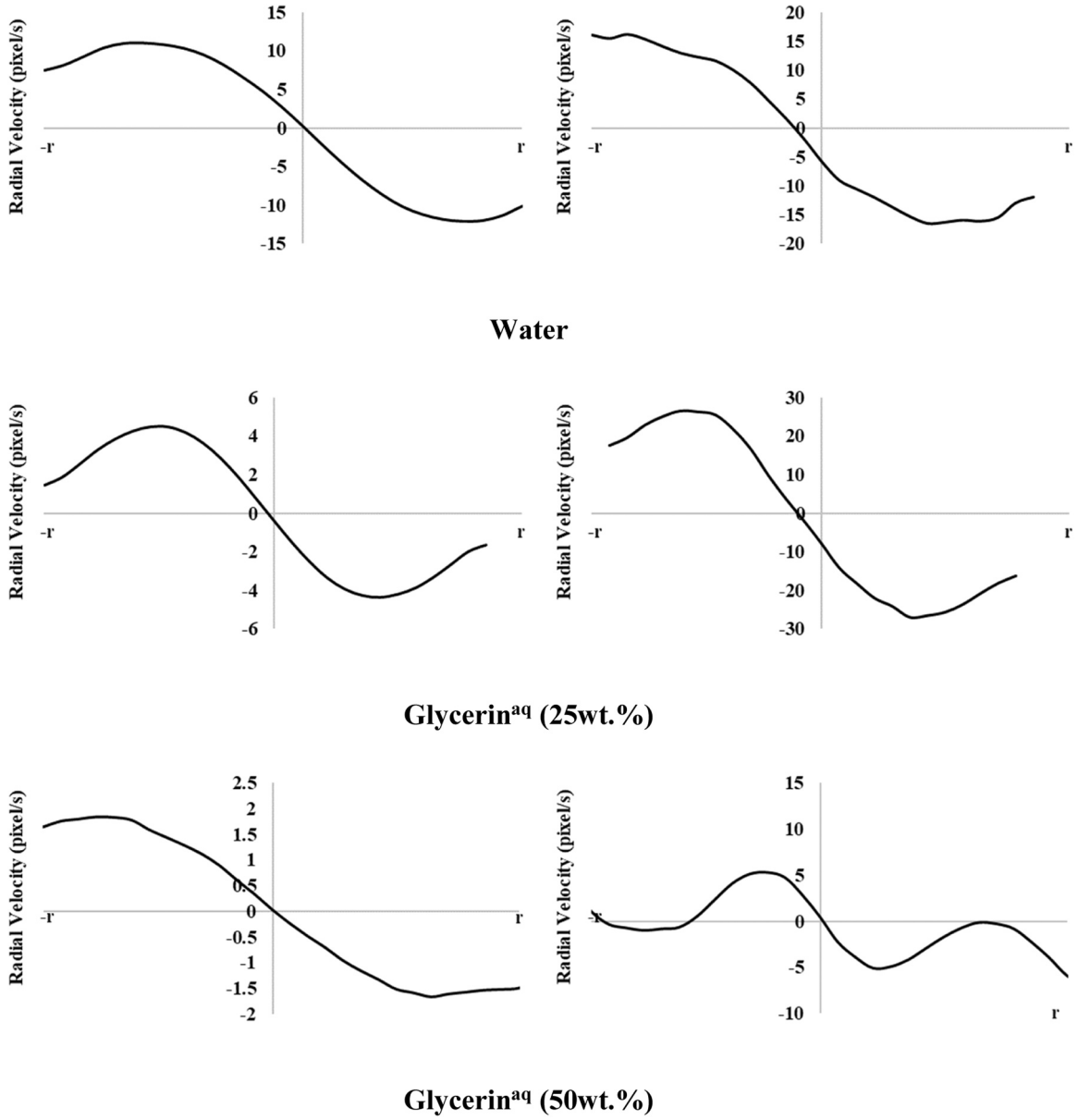

Fig. 7. Comparison of radial velocity profiles of stable ($Re<Re_c$) and unstable ($Re>Re_c$) flow regimes.

geometry at $10 \leq Re \leq 280$. Three sets of experiments including water and glycerin aqueous solutions of both 25 wt % and 50 wt % were employed to understand the effect of density and viscosity of the liquids on the liquid flow hydrodynamics. PLIF flow visualization and PIV measurements were performed to identify the liquid flow hydrodynamics. Formation of swirl behavior was observed at $Re = 40$ for water/water and glycerin^{aq}(25 wt %)/ glycerin^{aq}(25 wt %) and at Re=30 for glycerin^{aq}(50 wt %)/glycerin^{aq}(50 wt %) from radial plane measurements. Under this first turning point of the flow, from segregated to vortex flow, mixing was dominated by diffusion. As Re number increased, shear stress between fluid streams started to rule the flow. It was shown that the flow instabilities are first generated at around Re=220 for water/water and $Re = 200$ for glycerin^{aq}(25 wt %)/ glycerin^{aq}(25 wt %) and $Re = 170$ for glycerin^{aq}(50 wt %)/glycerin^{aq}(50 wt %). The evolution of the liquid flow hydrodynamics in the vortex mixer chamber was found to be very similar to the gas flow hydrodynamics. The linearly decreasing trend of the critical Re number based on the kinematic viscosity was found for liquids. Furthermore, kinematic viscosity was proven to be one of the most important factors affecting liquid flow hydrodynamics.

Declaration of Competing Interest

The authors declare that they have no known competing financial interests or personal relationships that could have appeared to influence the work reported in this paper.

Acknowledgements

This research did not receive any specific grant from funding agencies in the public, commercial, or not-for-profit sectors.

Supporting Information

Supporting information to this article can be found online at

References

Alboiu, E.F., Rus, S., Alboiu, N.I., Degeratu, M., 2017. Continuous flow type gas blending facility used for autonomous and system diving. Energy Procedia 112, 3–10. https://doi.org/10.1016/j.egypro.2017.03.1054.

Andersson, B., Andersson, R., Håkansson, L., Mortensen, M., Sudiyo, R., Van Wachem, B., 2011. Computational Fluid Dynamics for Engineers. Cambridge university press.

Ansari, M.A., Kim, K.-Y., Anwar, K., Kim, S.M., 2012. Vortex micro T-mixer with non-aligned inputs. Chem. Eng. J. 181, 846–850. https://doi.org/10.1016/j.cej.2011.11.113.

Ansari, M.A., Kim, K.-Y., Kim, S.M., 2018. Numerical and experimental study on mixing performances of simple and vortex micro T-mixers. Micromachines 9, 204. https://doi.org/10.3390/mi9050204.

Bie, H., Xue, L., Wang, Y., Liu, G., Hao, Z., An, W., 2022. Flow regimes and mixing performance in TT jet reactor. Chem. Eng. Process. Process. Intensif. 170, 108700 https://doi.org/10.1016/j.cep.2021.108700.

Brito, M., Barbosa, I., Fonte, C., Dias, M., Lopes, J., Santos, R., 2022a. Effective mixing of dissimilar fluids in asymmetric confined impinging Jets mixers. Chem. Eng. Sci. 258, 117756 https://doi.org/10.1016/j.ces.2022.117756.

Brito, M.S., Fonte, C.P., Dias, M.M., Lopes, J.C.B., Santos, R.J., 2022b. Flow regimes and mixing of dissimilar fluids in T-jets mixers. Chem. Eng. Technol. 45, 355–364. https://doi.org/10.1002/ceat.202100536.

Camarri, S., Mariotti, A., Galletti, C., Brunazzi, E., Mauri, R., Salvetti, M.V., 2020. An overview of flow features and mixing in micro T and arrow mixers. Ind. Eng. Chem. Res. 59, 3669–3686. https://doi.org/10.1021/acs.iecr.9b04922.

Chan, S.T., Ault, J.T., Haward, S.J., Meiburg, E., Shen, A.Q., 2019. Coupling of vortex breakdown and stability in a swirling flow. Phys. Rev. Fluids 4, 084701. https://doi.org/10.1103/PhysRevFluids.4.084701.

Cheng, J.C., Olsen, M.G., Fox, R.O., 2009. A microscale multi-inlet vortex nanoprecipitation reactor: turbulence measurement and simulation. Appl. Phys. Lett. 94 https://doi.org/10.1063/1.3125428.

Crimaldi, J., 2008. Planar laser induced fluorescence in aqueous flows. Exp. Fluids 44, 851–863. https://doi.org/10.1007/s00348-008-0496-2.

Gecim, G., Erkoc, E., 2021. Gas flow hydrodynamics in vortex mixers: flow visualization and PIV flow field characterization. Ind. Eng. Chem. Res. 60, 5674–5687. https://doi.org/10.1021/acs.iecr.1c00522.

Gecim, G., Erkoc, E., 2022. Hydrodynamics of similar gases in vortex mixers: effect of physical properties on the onset of instability. Ind. Eng. Chem. Res. 61, 1192–1206. https://doi.org/10.1021/acs.iecr.1c04387.

Hitimana, E., Fox, R.O., Hill, J.C., Olsen, M.G., 2019. Experimental characterization of turbulent mixing performance using simultaneous stereoscopic particle image velocimetry and planar laser-induced fluorescence. Exp. Fluids 60, 1–13. https://doi.org/10.1007/s00348-018-2669-y.

Hoffmann, M., Schlüter, M., Räbiger, N., 2006. Experimental investigation of liquid–liquid mixing in T-shaped micro-mixers using μ-LIF and μ-PIV. Chem. Eng. Sci. 61, 2968–2976. https://doi.org/10.1016/j.ces.2005.11.029.

Jin, L., Cao, Y., 2022. Coherent structures and mixing enhancement in a confined impinging-jet mixer. Chem. Eng. Sci. 262, 118014 https://doi.org/10.1016/j.ces.2022.118014.

Li, C., Wu, B., Zhang, J., Luo, P., 2022. Effect of swirling addition on the liquid mixing performance in a T-jets mixer. Chin. J. Chem. Eng. 50, 108–116. https://doi.org/10.1016/j.cjche.2022.07.008.

Li, H., Xu, D., 2023. An overview of fluids mixing in T-shaped mixers. Theor. Appl. Mech. Lett., 100466 https://doi.org/10.1016/j.taml.2023.100466.

Li, W.F., Du, K.J., Yu, G.S., Liu, H.F., Wang, F.C., 2014. Experimental study of flow regimes in three-dimensional confined impinging jets reactor. AIChE J. 60, 3033–3045. https://doi.org/10.1002/aic.14459.

Liu, Z., Hill, J.C., Fox, R.O., Olsen, M.G., 2014. Investigation of Turbulent Mixing in a Macro-Scale Multi-Inlet Vortex Nanoprecipitation Reactor by Stereoscopic-PIV. Fluids Engineering Division Summer Meeting. American Society of Mechanical Engineers. https://doi.org/10.1115/FEDSM2014-21976.

Liu, Z., Ramezani, M., Fox, R.O., Hill, J.C., Olsen, M.G., 2015. Flow characteristics in a scaled-up multi-inlet vortex nanoprecipitation reactor. Ind. Eng. Chem. Res. 54 (16), 4512–4525. https://doi.org/10.1021/ie5041836.

Mariotti, A., Antognoli, M., Galletti, C., Mauri, R., Salvetti, M.V., Brunazzi, E., 2020. The role of flow features and chemical kinetics on the reaction yield in a T-shaped micro-reactor. Chem. Eng. J. 396, 125223 https://doi.org/10.1016/j.cej.2020.125223.

Rabani, R., Talebi, S., Rabani, M., 2016. Numerical analysis of lamination effect in a vortex micro T-mixer with non-aligned inputs. Heat. Mass Transf. 52, 611–619. https://doi.org/10.1007/s00231-015-1584-5.

Santos, R.J., Erkoç, E., Dias, M.M., Teixeira, A.M., Lopes, J.C.B., 2008. Hydrodynamics of the mixing chamber in RIM: PIV flow-field characterization. AIChE J. 54, 1153–1163. https://doi.org/10.1002/aic.11472.

Shen, B., Zhan, X., Sun, Z., He, Y., Long, J., Li, X., 2022. PIV experiments and CFD simulations of liquid–liquid mixing in a planetary centrifugal mixer (PCM). Chem. Eng. Sci. 259, 117764 https://doi.org/10.1016/j.ces.2022.117764.

Shi, Y., Fox, R.O., Olsen, M.G., 2011. Confocal imaging of laminar and turbulent mixing in a microscale multi-inlet vortex nanoprecipitation reactor. Appl. Phys. Lett. 99 https://doi.org/10.1063/1.3662042.

Sultan, M.A., Fonte, C.P., Dias, M.M., Lopes, J.C.B., Santos, R.J., 2012. Experimental study of flow regime and mixing in T-jets mixers. Chem. Eng. Sci. 73, 388–399. https://doi.org/10.1016/j.ces.2012.02.010.

Valdés, J.P., Kahouadji, L., Matar, O.K., 2022. Current advances in liquid–liquid mixing in static mixers: a review. Chem. Eng. Res. Des. 177, 694–731. https://doi.org/10.1016/j.cherd.2021.11.016.

Wu, B., Li, C., Zhang, M., Luo, P., 2021. Liquid mixing intensification by adding swirling flow in the transverse jet mixer. AIChE J. 67, e17276 https://doi.org/10.1002/aic.17276.

Xia, Q., Zhong, S., 2013. Liquids mixing enhanced by multiple synthetic jet pairs at low reynolds numbers. Chem. Eng. Sci. 102, 10–23. https://doi.org/10.1016/j.ces.2013.07.019.

Xiang, J., Li, Q., Tan, Z., Zhang, Y., 2017. Characterization of the flow in a gas-solid bubbling fluidized bed by pressure fluctuation. Chem. Eng. Sci. 174, 93–103. https://doi.org/10.1016/j.ces.2017.09.001.

Zhang, W., Zhang, J.-w, Li, W.-f, Liu, H.-f, Wang, F.-c, 2020. Flow regimes and mixing characteristics in non-aligned T-jets reactors. Chem. Eng. Sci. 228, 115991 https://doi.org/10.1016/j.ces.2020.115991.